https://doi.org/10.48048/tis.2023.5827

Identification of Mountain Waves and Their Characteristics in the Central Java Region based on the WRF Numerical Weather Model

Aries Kristianto[1,*], Fara Diva Claudia[2] and Rista Hernandi Virgianto[3]

[1]Department of Meteorology, School of Meteorology Climatology and Geophysics, Tangerang Selatan 15221, Indonesia
[2]Teluk Bayur Meteorological Station, Agency for Meteorology Climatology and Geophysics, Padang 25123, Indonesia
[3]Department of Climatology, School of Meteorology Climatology and Geophysics, Tangerang Selatan 15221, Indonesia

([*]Corresponding author's e-mail: aries.kristianto@stmkg.ac.id)

Received: 31 August 2022, Revised: 25 October 2022, Accepted: 3 March 2023, Published: 1 August 2023

Abstract

One of the factors that influence the complexity of the weather and climate phenomena in Indonesia is the diverse topographical conditions. The Mountain waves are quite common in Indonesia, especially on the island of Java, which has several mountains with quite high peaks. The existence of mountain waves can be known from the presence of lenticularis clouds both on top of the mountain are regularly reported by residents in the area of Mount Ungaran and Mount Lawu in Centra Java. This study utilized the Weather Reasearch Forecast (WRF), a numerical weather model to identify mountain waves and their characteristics in Mount Ungaran and Mount Lawu. The results of the study are that there were 2 mountain wave events in Mount Ungaran on 9 September 2018 with an average duration of 5 h, and horizontal wavelengths reaches 28 km. During that mountain wave events, there was also a type 1 rotor with dominant positive vorticity and a breaking pattern that indicates the potential for strong turbulence which is supported by critical Ri value at a distance of 30 - 90 m on the leeward side. Meanwhile, in Mount Lawu case on 9 March 2019, the mountain wave onset occurs during the day is in the afternoon, its duration is 2 h, wavelengths ranging from 5.9 to 6.1 km, where in the leeward side has no strong turbulence potential. In general, WRF can simulate both mountain waves and rotors, but has not been able to properly simulate the downslope windstorms.

Keywords: Mountain wave, Rotor, Downslope windstorm, Vertical wind shear, Richardson number, Froude number, WRF

Introduction

Mountain waves are atmospheric waves that occur when strong winds pass through a topographical obstacle with the normal wind component perpendicular to the barrier [1]. Basically, mountain waves occur due to strong wind that hit topographical barriers and lead to the top when atmospheric conditions are stable, then generate turbulence when they reach the other side of the mountain known as the leeward side [2,3]. Mountain waves are generally considered a small-scale meteorological phenomenon. However, wind-flow over broad ridges can produce orographic disturbances in the meso-scale range of 10 to 100 km, which characteristics depend on windspeed averages and stability profiles [4].

Indonesia as an archipelago located in the maritime continent has complexities in weather and climate phenomena [5-7]. One of many factors that influence the complexity is the diverse topographic conditions consisting of lowlands, highlands and mountains with high peaks [8]. Lenticularis clouds form within the crest of these mountain waves where the air is ascending when there is enough moisture above mountain-top level [1]. Mount Lawu and Mount Ungaran are some of the mountains on the central part of Java reported by local residents that lenticular clouds are often seen.

When a mountain wave produces a very high amplitude, it will form a windstorm that descends the mountain slope called downslope windstorm. This windstorm may cause an extensive damage to the slopes of the mountains because of its high wind speeds [9-11]. In addition, the high amplitude of mountain waves can lead to the formation of a rotor circulation near the surface, when the flow reverses a short distance horizontally, the flow breaks and then rotates with height [12,13]. The type of rotor depends on the sign of

the dominant horizontal vorticity with positive vorticity dominate the developing type 1 rotor, while negative vorticity dominate the developing type 2 rotor [14].

Research related to mountain waves in Indonesia is still limited because of the lack of in-situ observation data in mountainous areas. To overcome this lack of observation data, research on mountain waves can be carried out based on reanalyzed data processed using numerical weather models such as Weather Research and Forecasting (WRF) model [15,16]. Based on the aforementioned background, this study aims to analyze the occurrence of mountain waves using the WRF model, when the lenticular clouds of Mount Ungaran and Mount Lawu are reported to be visible to local residents.

Materials and methods

The research locations in this study are Mount Ungaran and Mount Lawu that located in Central Java, which are shown in **Figure 1**. Mount Ungaran, which rises to a height of 2,050 m above ground level (AGL), is situated south of Central Java's northern coast, whereas Mount Lawu, a sizable compound stratovolcano that stands at 3,265 m AGL, is situated between Central and East Java in Indonesia [17]. The time of the research was carried out based on a case study on 9 September 2018 when a downslope windstorm occurred on Mount Ungaran and on 9 March 2019 on Mount Lawu. Some residents around the mountain at that time reported the presence of lenticular clouds seen above the peaks of Mount Ungaran and Mount Lawu [18,19].

The synoptic observation data used in this study include direction and speed of the surface wind, temperature and humidity used as a comparison in verifying the WRF simulations. Meteorological data were obtained from The Agency for Meteorology, Climatology and Geophysics of The Republic of Indonesia (BMKG). A 6 h time interval of Final Data Analysis (FNL) from National Centers for Enviromental Prediction (NCEP) used to generate the initial conditions in the WRF-ARW [20]. The FNL dataset is in GRIB2 format with a grid resolution of 0.25 ° (~27.75 km) and downloaded on https://rda.ucar.edu/datasets/ds083.3/. We used 48 h of running period in WRF model, included 24 h of spin up time with 1 km^2 resolution for each case using the configuration as shown in **Table 1**.

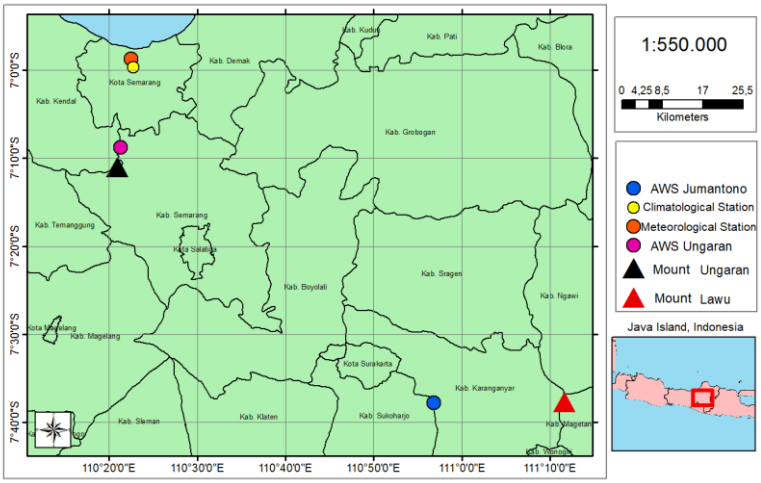

Figure 1 Research locations on Mount Ungaran and Mount Lawu, Central Java.

Table 1 Configuration of the WRF-ARW model used in this study.

Configuration	Domains		
	d1	d2	d3
Horizontal resolution	9 km	3 km	1 km
Domains time step	60 s	60 s	60 s
Physics suite	tropical	tropical	tropical
Cumulus parameterization	0 (off)	0 (off)	0 (off)
Cumulus parameterization	0 (off)	0 (off)	0 (off)

The potential temperature parameters and geopotential height from the WRF simulation were used to calculate the Brunt-Väisälä frequency (N) by using following formula [21]:

$$N = \sqrt{\frac{g}{\theta}\frac{d\theta}{dz}} \quad (1)$$

with θ is potential temperature (K); g is gravity acceleration constant (9.8 m/s^2); z is geopotential height (m). The value of the Brunt-Väisälä frequency, surface wind speed and the height of the mountain peak were used to calculate the Froude number (Fr) [22], which is formulated by:

$$Fr = \frac{U}{Nh} \quad (2)$$

with U is the surface wind speed over mountains (m/s); N is Brunt-Väisälä frequencies representing static stability; h is the mountain peak height (m).

Brunt-Väisälä frequency values, Fr, and temporal analysis of vertical velocity were used to determine the onset and dissipation of mountain waves [23]. If the value of $Fr > 1$, it indicates that there is oscillation so that there is mountain wave activity and if the value of $Fr < 1$, it indicates that there is no oscillation so that there is no mountain wave activity [22]. Determination of mountain wavelengths is based on spatial analysis of vertical velocity using the WRF model and linear wave calculations [24,25].

Rotor characteristics and downslope windstorm were determined by analyzing the value of horizontal vorticity [13]. The relationship of VWS in the inversion layer and horizontal wind speed at the top of the mountain was used to determine the type of rotor that occurred [14,26]. The turbulence potential generated by the rotor is obtained based on the Ricardson number (Ri). In a moderate turbulence, the Ri value is higher than 0.25 and lower than 1, while for a high turbulence if the Ri value is lower than 0.25. The wind parameters from the model output are used to see the wind speed on the slopes of the mountain. In addition, the classification of mountain waves is obtained based on cross section analysis of vertical wind speed around the mountain during the occurrence of mountain waves. We determine the characteristics of downslope windstorms by analyzing the isentropic contours and wind speed on top of the mountain peak. A value of Ri less than 0.25 denoting the presence of a strong turbulent flow on the mountain slopes [27].

Results and discussion

WRF verification

The reliability and accuracy of the WRF numerical simulations were verified with weather parameters observed with nearest Automatic Weather Stations (AWS Ungaran), synoptic observation data in meteorological station (MS) and climatological station (CS) which locations as in **Figure 1**. The simulation in Mount Ungaran case using WRF model started from 07.00 LT on 8 September 2018 to 07.00 LT on 9 September 2018. **Table 2** shows the verification results of the WRF simulation.

Table 2 The verification results of WRF simulation on 9 September 2018 at some observation points for Mount Ungaran case.

Parameters	Correlation			RMSE		
	AWS Ungaran	MS	CS	AWS Ungaran	Met Station	Clim Station
Air temperature	0.537	0.290	0.817	18.781	5.987	2.722
Air humidity	0.547	0.326	0.543	5.285	11.117	15.423
Wind velocity	0.274	0.573	0.142	5.322	2.606	3.923
Air pressure	0.309	0.196	0.367	13.426	2.138	7.807

Verification on 9 September 2018 shows that the surface air temperature element has a correlation value greater than 0.5 and a relatively low RMSE value. The air humidity element has a fairly good correlation value but the RMSE value is not good enough, which is greater than 10. In the verification of the wind speed and air pressure elements, the correlation value is less than 0.5. However, the RMSE values for the elements of wind speed and air pressure are relatively low, indicating that the WRF model can still simulate surface wind elements even though the results are not good enough. Analysis of correlation values

and RMSE in **Table 2**, shows that the use of the Tropical Scheme in this WRF simulation is quite good in simulating the elements of temperature and humidity of the surface air, but not good enough in simulating the elements of surface wind and air pressure in Mount Ungaran case.

We used nearest AWS (AWS Jumantono) in verification of the WRF simulation in Mount Lawu case. The simulation was started from 07.00 LT on 8 March 2019 to 07.00 LT on 9 March 2019. Based on **Table 3**, the verification results showed a very strong correlation value with the results of observations from AWS in air temperature and humidity. This shows that the WRF model well simulate the air temperature and humidity in Mount Lawu. Meanwhile in wind speed and air pressure, the correlation value is less than 0.5, which means that both parameters have a weak correlation. The RMSE value of the wind speed simulation is relatively low, while RMSE of the air pressure simulation is the highest among all parameters. Analysis of correlation and RMSE shows that the use of the Tropical Scheme in the WRF simulation is quite good in simulating the elements of surface air temperature and humidity, but not good enough in simulating the elements of surface wind and air pressure in Mount Lawu case.

WRF simulations give better results on surface air temperatures because the use of the 'tropical suite' parameterization scheme which is also in other studies in Indonesia is indeed suitable for simulating surface air temperatures in the tropics [28]. In addition, the WRF simulation in this study also showed reliable results in the air humidity simulation. This is in line with another research in Indonesia by Hastuti and Paski [29], that also used a 'tropical suite' parameterization which still gave reliable outcomes in simulating air humidity even without data assimilation. However, the WRF simulation in this study gave unsatisfactory results in simulating surface wind speed and surface pressure. The difficulty of the WRF model in simulating surface wind and surface air pressure is also experienced in another research in Indonesia by Sari *et al.* [30], which also use WSM6 contained in the 'tropical suite' as a microphysics scheme in their WRF model.

Table 3 The verification results of WRF simulation on 9 March 2019 at AWS Jumantono on Mount Lawu case.

Accuracy parameters	**Correlation**	**RMSE**
	AWS Jumantono	**AWS Jumantono**
Air temperature	0.701	1.926
Air humidity	0.642	15.251
Wind velocity	0.301	6.271
Air pressure	0.287	24.231

Mountain wave analysis

The results of a linear calculation on 9 September 2018 at Mount Ungaran are shown in **Table 4** which indicates that the waves have the potential to oscillate when passing through the mountain at a layer of 500 mb, with a value of N^2 more than 0 from 07.00 to 24.00 Local Time (LT). The 500 mb layer is used in mountain wave analysis because between these layers lenticular clouds usually observed above the mountain peaks as a sign of mountain waves existence [31]. In the first mountain wave event, the wave onset was known from the value of Fr more than 1 at 01.00 LT, which then the mountain wave dissipated at 07.00 LT. In the second incident, the onset of the mountain wave occurred at 13.00 LT and then dissipated at 23.00 LT.

Table 4 Characteristics of the 500 mb layer mountain waves based on linear calculations on 9 September 2018 at Mount Ungaran.

LT	Brunt-Väisälä frequency (s^{-1})	N^2 (s^{-2})	Fr (s^{-1})	Horizontal wavelength (km)	Wave classification
00	0.01213	0.0001471	0.56	-	-
01	0.01242	0.0001541	1.10	5.0	Vertically propagating wave
02	0.01223	0.0001495	1.10	4.8	Vertically propagating wave
03	0.01199	0.0001438	1.02	5.0	Vertically propagating wave
04	0.01166	0.0001359	1.03	5.1	Vertically propagating wave
05	0.01172	0.0001373	1.01	5.4	Vertically propagating wave
06	0.01165	0.0001356	1.01	5.4	Vertically propagating wave
07	0.01189	0.0001413	1.02	5.2	Vertically propagating wave
08	0.01146	0.0001313	1.03	5.3	Vertically propagating wave
09	0.01190	0.0001415	0.66	-	-
10	0.01233	0.0001521	0.67	-	-
11	0.01214	0.0001475	0.67	-	-
12	0.01211	0.0001467	0.65	-	-
13	0.01220	0.0001489	1.00	6.8	Vertically propagating wave
14	0.01228	0.0001507	1.04	7.0	Vertically propagating wave
15	0.01220	0.0001489	1.02	6.4	Vertically propagating wave
16	0.01221	0.0001492	1.07	7.1	Vertically propagating wave
17	0.01291	0.0001666	1.03	6.7	Vertically propagating wave
18	0.01300	0.0001689	1.03	6.8	Vertically propagating wave
19	0.01310	0.0001716	1.03	6.6	Vertically propagating wave
20	0.01321	0.0001745	1.03	6.7	Vertically propagating wave
21	0.01321	0.0001744	1.02	6.8	Vertically propagating wave
22	0.01328	0.0001764	1.003	6.9	Vertically propagating wave
23	0.01320	0.0001742	1.07	6.9	Vertically propagating wave
24	0.01314	0.0001727	0.95	-	-

Based on **Figure 2**, the occurrence of mountain wave oscillations on 9 September 2018 was fluctuated. On that day there were 3 occurrences of mountain waves that appeared and dissipated. In the first incident, the onset of the mountain wave started at 07.00 LT and dissipated at 10.00 LT. Mountain waves on the first occurrence can oscillate for up to 2 h. In the second incident, the onset of the mountain wave occurred at 12.00 LT, then the wave strengthened at 16.00 LT which was marked by an increase in vertical speed and an increase in wave amplitude and then the wave weakened at 19.00 LT, which was indicated by a weakening vertical velocity value, and the wave amplitude is also weakened, but the wave propagation horizontally has expanded until mountain waves dissipate at 22.00 LT.

Two mountain wave events were identified on 9 September 2018 at Mount Ungaran. The duration of the occurrence of the first mountain wave is 6 h, while the duration of the occurrence of the second mountain wave is 10 h. The mountain wave oscillates as far as 4.8 to 7.1 km horizontally. The classification of mountain waves obtained from on cross section analysis of vertical wind speed around the mountain is vertically propagating wave (**Figure 2**). The duration of the oscillating mountain wave on 9 September

2018 can last from 8 to 11 h. The presence of 2 mountain waves on Mount Ungaran in the morning and evening suggests that the mountain waves were moved between but did not move for several hours. This shifting can result from a wavelength shortening in the afternoon caused by a slowing of the upstream horizontal wind speed [32].

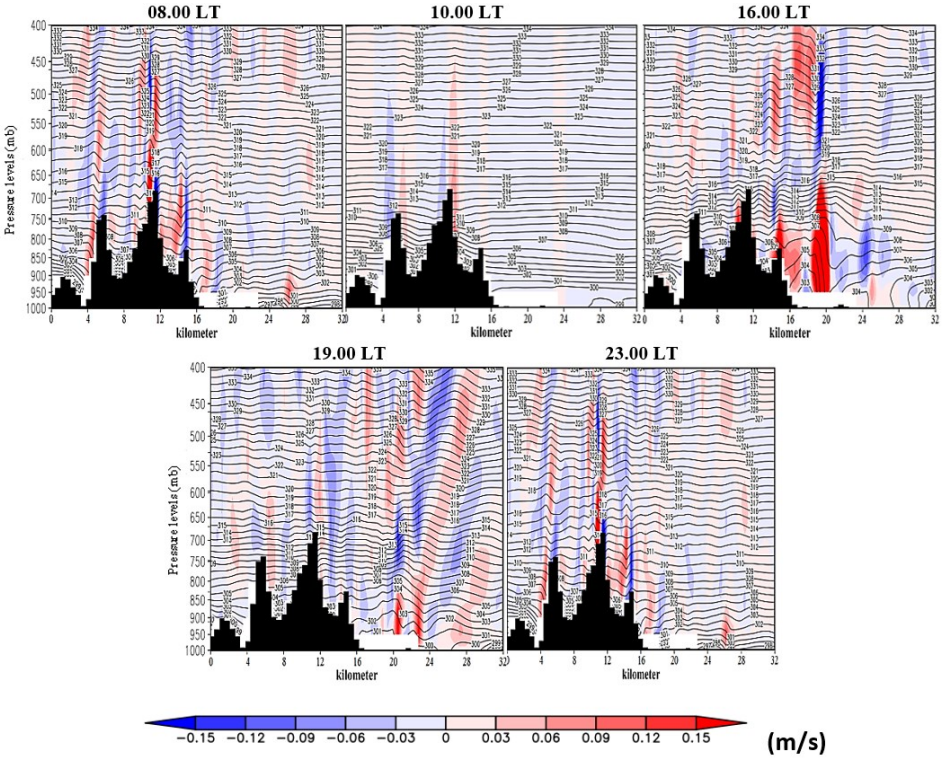

Figure 2 Vertical air velocity (m/s) and isentropic contour near Mount Ungaran on 9 September 2018 with the contour line refers to potential temperature in K.

Meanwhile in Mount Lawu case, the characteristics of mountain waves based on the results of linear calculations on 9 March 2019 shown in **Table 5**, it was found that the wave onset occurred at 13.00 LT and dissipated at 15.00 LT. The duration of the mountain waves on that day was 2 h, with wavelengths ranging from 5.9 to 6.1 km, and were classified as vertically propagating waves.

Table 5 Characteristics of the 500 mb layer mountain waves based on linear calculations on 9 March 2019 at Mount Lawu.

LT	Brunt-Väisälä frequency (s^{-1})	N^2 (s^{-2})	Fr (s^{-1})	Horizontal wavelength (km)	Wave classification
00	0.01300	0.00002	0.6	-	-
01	0.00567	0.0000322	1.06	4.2	-
02	0.00733	0.0000537	0.78	-	-
03	0.00701	0.0000492	0.78	-	-
04	0.00708	0.0000501	0.78	-	-
05	0.00701	0.0000492	0.839	-	-
06	0.00692	0.0000479	0.89	-	-
07	0.00685	0.0000469	0.97	-	-
08	0.03013	0.0000671	0.22	-	-

LT	Brunt-Väisälä frequency (s^{-1})	N^2 (s^{-2})	Fr (s^{-1})	Horizontal wavelength (km)	Wave classification
09	0.00694	0.0000679	0.92	-	-
10	0.00665	0.0000630	0.96	-	-
11	0.00653	0.0000580	0.97	-	-
12	0.00649	0.0000539	0.95	-	-
13	0.00622	0.00004974	1.14	5.9	Vertically propagating wave
14	0.00645	0.00005073	1.13	5.9	Vertically propagating wave
15	0.00655	0.0001074	1.01	6.1	Vertically propagating wave
16	0.00659	0.0001080	0.97	-	-
17	0.00666	0.0000460	0.91	-	-
18	0.00682	0.0000433	0.96	-	-
19	0.00677	0.0000928	0.96	-	-
20	0.00668	0.0000515	0.89	-	-
21	0.00749	0.0000514	0.91	-	-
22	0.00748	0.0000536	0.92	-	-
23	0.00755	0.0000542	0.90	-	-
24	0.00770	0.0000563	0.95	-	-

Based on the vertical velocity analysis, the onset of the mountain wave on 9 March 2019 as shown in **Figure 3**, started at 13.00 LT, and dissipated at 15.00 LT. Then the mountain wave oscillates with the duration of 2 h on that day. Horizontal mountain wavelengths can reach 4 km. Vertical wave oscillations based on spatial vertical velocity analysis show oscillating waves up to 600 mb layer.

The analysis of vertical wind speed and isentropic contours shows that the mountain waves on Mount Ungaran and Lawu are vertically propagating waves in both cases. There was slight wind shear direction between the upper and lower pressure levels in both cases. Because the lack of such wind shear prevents the formation of critical levels in the atmosphere, which can obstruct wave propagation upward. This will help the formation and vertical propagation of mountain waves [33].

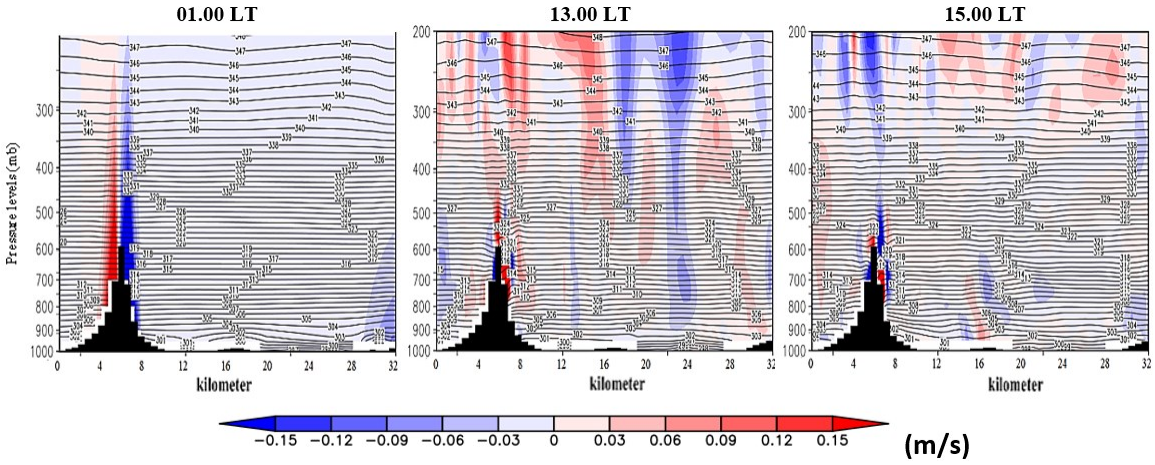

Figure 3 Vertical air velocity (m/s) and isentropic contour near Mount Lawu on 9 March 2019 with the contour line refers to potential temperature in K.

The characteristics of the mountain wave rotor on Mount Ungaran are shown in **Figure 4**, where there was a breaking wave pattern indicated by a strong turbulence at that location on 9 September 2018. This is supported by the negative and positive vorticity value which also dominates the area. At 19.00 LT, the value of the vorticity weakened and there was no longer a breaking wave pattern, while there was a tight isentropic contour. In general, the horizontal vorticity at the time of the occurrence of mountain waves has a positive value of 0.2 to more than1 s^{-1}. However, at 16.00 LT, there was a negative horizontal vorticity with a value of −0.2 to −0.4 s^{-1}. Rotor activity can expand up to 650 mb layer.

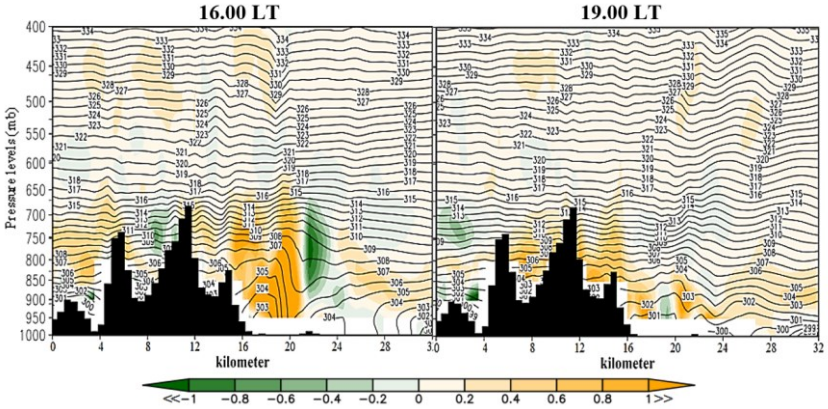

Figure 4 Horizontal air vorticity (s^{-1}) on 9 September 2018 at Mount Ungaran with the contour line refers to potential temperature in K.

Based on **Figure 5**, on the leeward side of the Mount Ungaran there is a Ri value less than 1 at 16.00 LT. This indicates the potential for turbulence at that location. At a height of z2 there is a critical Ri value (Ri ≤ 0.25) which indicates a strong potential for turbulence at that altitude [27]. The potential for strong turbulence extends to an altitude of z = 4.5 km. Meanwhile, at 19.00 LT on the leeward side of the mountain, a pattern of the Ri value was seen which was the same as the Ri value at 16.00 LT. This is due to the presence of a dense isentropic contour even though the intensity of the vorticity value is weakened. Based on the results, in general, the rotor produced was a type 1 rotor with a dominant positive vorticity value [14]. Moreover, during 16.00 LT, at a height of z2 there is a critical Ri value (Ri ≤ 0.25) which also indicates a strong potential for turbulence at that altitude.

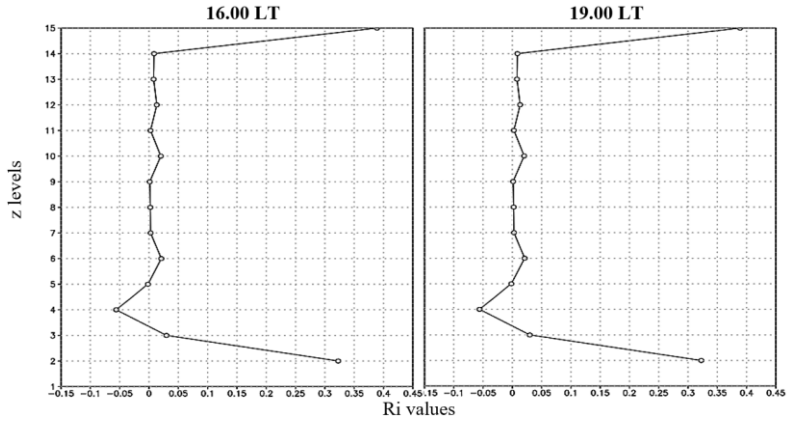

Figure 5 Richardson Numbers (Ri) to determine turbulent flow when the rotor occurs on 9 September 2018 at Mount Ungaran with each value of z level = 30 m.

At 13.00 LT, on the leeward side of the Mount Lawu, there is a Ri value of more than 1 at an altitude of z1. This indicates that there is no potential for turbulence at this location. The low Ri value (0.5 ≤ Ri ≤ 1) starts to show at the 900 mb layer. Then when z2 there is a subcritical Ri value (0.25 ≤ Ri ≤ 0.5) and a low Ri value which indicates a potential for weak to moderate turbulence [27]. Then at an altitude where there is a wave pattern on the isentropic contour (overturning isentropic), there is a critical Ri value (Ri ≤ 0.25) which indicates a strong turbulence potential at that altitude [27]. Meanwhile, at 14.00 LT the critical

Ri value (Ri ≤ 0.25) which indicates the potential for strong turbulence has begun to be seen in the 900 mb layer (**Figure 6**).

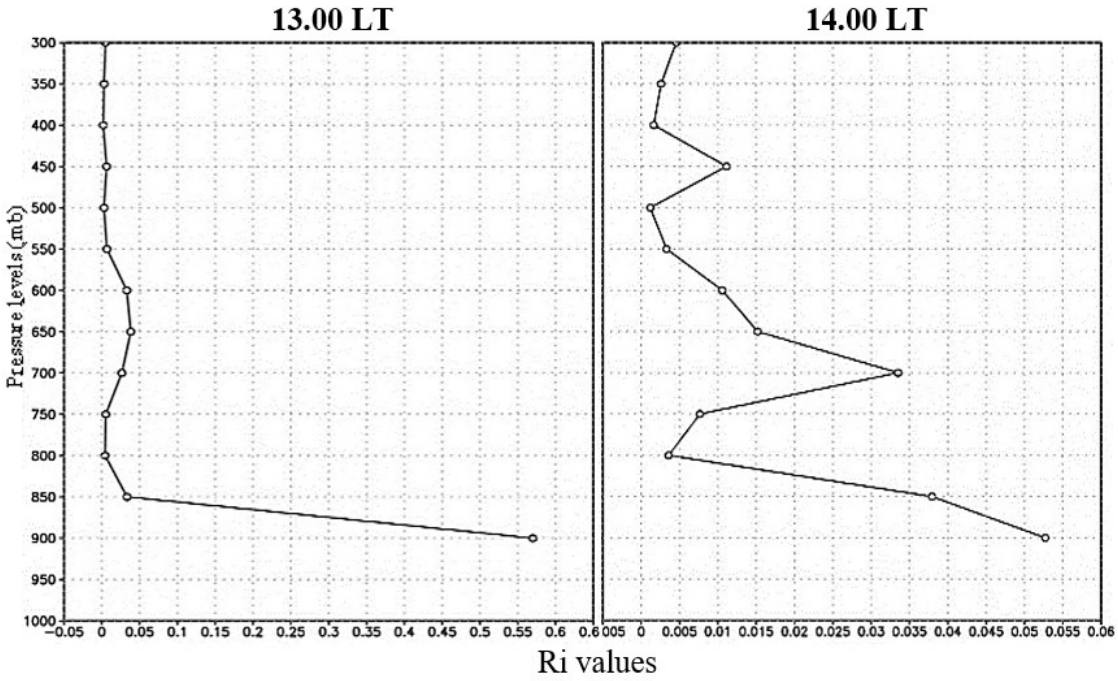

Figure 6 Richardson Number (Ri) to determine turbulent flow when a rotor occurs on 9 March 2019 at Mount Lawu.

Figure 7 shows the downslope characteristics of mountain wave windstorms in the Mount Ungaran. On that day there were 2 events of mountain waves that appeared and then dissipated. In the first incident, the onset of the mountain wave started at 07.00 LT and dissipated at 10.00 LT. Mountain waves on the first occurrence can oscillate for up to 2 h. In the second incident, the onset of the mountain wave occurred at 12.00 LT, then the wave strengthened at 16.00 LT which was marked by an increase in vertical speed and an increase in wave amplitude. The wave weakened at 19.00 LT, which was indicated by a weakening vertical velocity value and the wave amplitude is also weakened. However, the wave propagation horizontally has expanded and then dissipate at 22.00 LT.

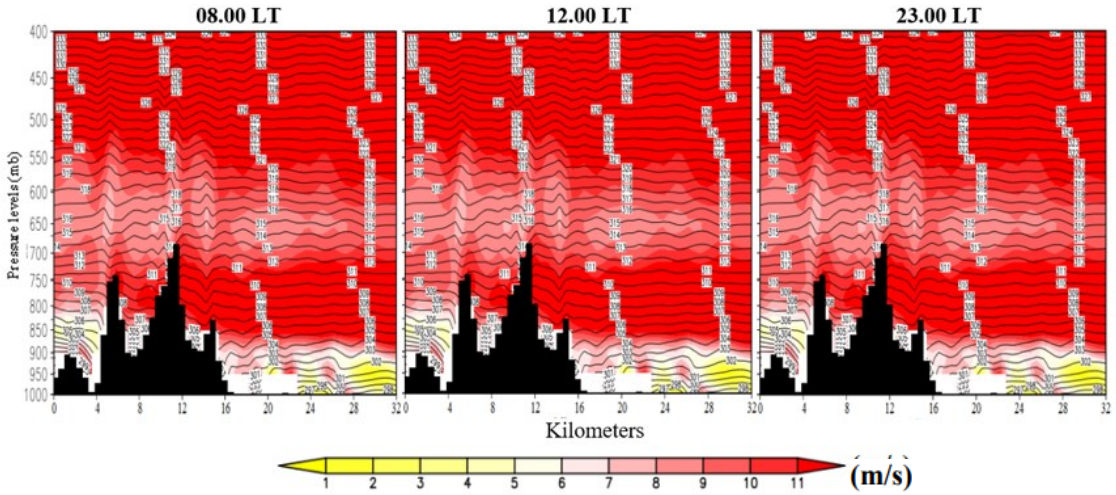

Figure 7 Wind speed and isentropic contours to determine the downslope windstorm during mountain wave on 9 September 2018 at Mount Ungaran with the contour line refers to potential temperature in K.

During the mountain waves on 9 March 2019 at Mount Lawu, there was no downslope windstorm on the slopes of the mountain. This is evidenced by the wind speed value of 3 to 5 m/s. In addition, on that day, both at 13.00 and 14.00 LT, no tight isentropic contours were seen on the side of the mountain slope (**Figure 8**).

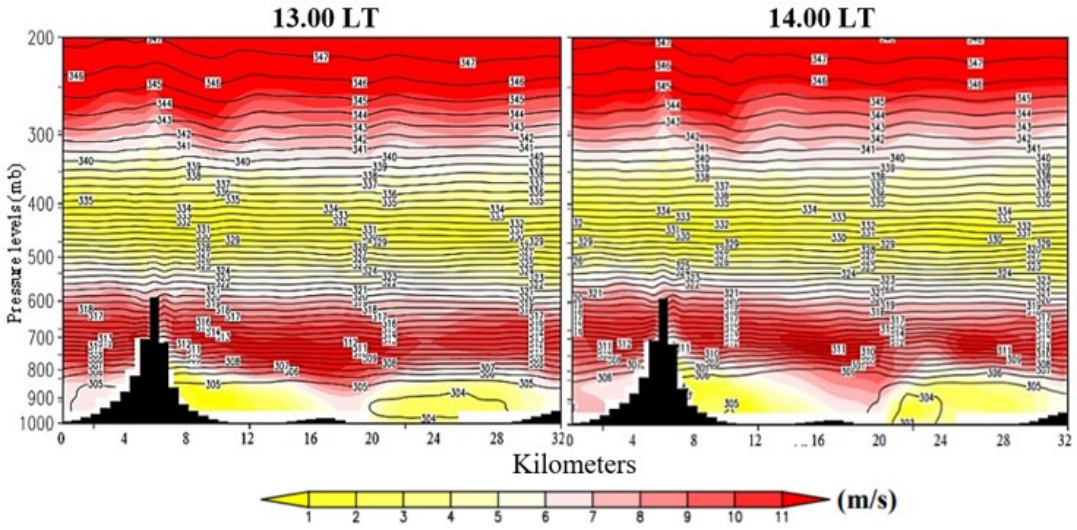

Figure 8 Wind speed and isentropic contours to determine the downslope windstorm during mountain waves on 9 March 2019 at Mount Lawu with the contour line refers to potential temperature in K.

Conclusions

In Mount Ungaran case on 9 September 2018, there was 2 mountain waves that appears and then dissipates. In the first incident, the onset of the mountain wave started in the morning and dissipated at 10.00 LT with oscillation duration up to 2 h. In the second incident, the onset of mountain waves occurred at noon and experienced a strengthening in the afternoon which was marked by an increase in the vertical speed. There was an increase in wave amplitude and then the waves weakened towards the evening marked by a weakened vertical velocity value with the amplitude also weakened. However, the wave propagation horizontally expanded, and finally dissipated at 22.00 LT. Meanwhile in Mount Lawu case on 9 March 2019, the onset of waves occurred during the day and then dissipated in the afternoon. The mountain waves last for 2 h with wavelengths ranging from 5.9 to 6.1 km.

The existence of a rotor on Mount Ungaran was indicated by the presence of a breaking wave pattern indicated by isentropic contours and horizontal vorticity with a type 1 rotor with strong turbulence. Meanwhile, in Mount Lawu case, on the leeward side of the mountain, there was no potential for turbulence at that location, while the 900 mb layer indicated the potential for weak to moderate turbulence. WRF can simulate mountain and rotor waves well, but could not well simulate the downslope windstorm on Mount Ungaran and Mount Lawu.

Acknowledgements

We would like to express our sincere gratitude to the board of the School of Meteorology Climatology and Geophysics (STMKG) for their funding support. Additionally, we extend our thanks to the Agency for Meteorology Climatology and Geophysics of the Republic of Indonesia (BMKG), specifically the Ahmad Yani Meteorological Station and Central Java Climatology Station for giving access to meteorological observation data used in this study. Furthermore, we thank all the anonymous reviewers.

References

[1] J Kuettner and CF Jenkins. *Flight aspects of the mountain wave.* Air Force Cambridge Research Center, Massachusetts, 1953.

[2] DR Durran and JB Klemp. The effects of moisture on trapped mountain lee waves. *J. Atmos. Sci.* 1982; **39**, 2490-506.

[3] DR Durran. Mountain waves and downslope winds. *Meteorol. Monogr.* 1990; **23**, 59-81.

[4] JR Holton and GJ Hakim. *An introduction to dynamic meteorology.* Academic Press, Cambridge, Massachusetts, 2013.

[5] HKB Tjasyono, R Gernowo, BSH Woro and J Ina. The character of rainfall in the Indonesian monsoon. *In*: Proceedings of the International Symposium on Equatorial Monsoon System, Yogyakarta, Indonesia. 2008.

[6] K Yoneyama and C Zhang. Years of the maritime continent. *Geophys. Res. Lett.* 2020; **47**, e87182.

[7] S Yang, T Zhang, Z Li and S Dong. Climate variability over the Maritime Continent and its role in global climate variation: A review. *J. Meteorol. Res.* 2019; **33**, 993-1015.

[8] TDF Hutapea, R Kurniawan and W Hanggoro. Pengaruh Topografi dan Luas Daratan Model WRF terhadap Hasil Prediksi Temperatur Permukaan Di Wilayah Kepulauan Indonesia (*in Indonesian*). *Jurnal Meteorologi Geofisika* 2015; **16**, 179-87.

[9] J Doyle and M Shapiro. A multi-scale simulation of an extreme downslope windstorm over complex topography. *Meteorol. Atmos. Phys.* 2000; **74**, 83-101.

[10] WY Sun. Numerical study of severe downslope windstorm. *Weather Clim. Extremes* 2013; **2**, 22-30.

[11] H Kusaka and H Fudeyasu. Review of downslope windstorms in Japan. *Wind Struct. Int. J.* 2017; **24**, 637-56.

[12] G Shutts. Gravity-wave drag parametrization over complex terrain: The effect of critical-level absorption in directional wind-shear. *Q. J. Roy. Meteorol. Soc.* 1995; **121**, 1005-21.

[13] JD Doyle and DR Durran. The dynamics of mountain-wave-induced rotors. *J. Atmos. Sci.* 2002; **59**, 186-201.

[14] RF Hertenstein and JP Kuettner. Rotor types associated with steep lee topography: Influence of the wind profile. *Tellus Dyn. Meteorol. Oceanogr.* 2005; **57**, 117-35.

[15] S Kirkwood, M Mihalikova, T Rao and K Satheesan. Turbulence associated with mountain waves over Northern Scandinavia - a case study using the ESRAD VHF radar and the WRF mesoscale model. *Atmos. Chem. Phys.* 2010; **10**, 3583-99.

[16] J Díaz-Fernández, L Quitián-Hernández, P Bolgiani, D Santos-Muñoz, Á García Gago, S Fernández-González, F Valero, A Merino, E García-Ortega, JL Sánchez, M Sastre and ML Martín. Mountain waves analysis in the vicinity of the Madrid-Barajas airport using the WRF model. *Adv. Meteorol.* 2020; **2020**, 8871546.

[17] E Venzke. *Global volcanism program. Volcanoes of the world, v. 4.11.2 (02 Sep 2022).* Smithsonian Institution, Washington, 2013.

[18] SoloPos. Fakta di Balik Keindahan Awan Mirip UFO Gunung Ungaran: Liputan6 (*in Indonesian*), Available at: https://www.liputan6.com/regional/read/3642273/fakta-di-balik-keindahan-awanmirip-ufo-gunung-ungaran, accessed June 2022.

[19] Kompas. Cantiknya Gunung Lawu Pagi Ini, Puncaknya Tampak Bertopi: Kompas (*in Indonesian*), Available at: https://regional.kompas.com/read/2019/10/03/08461781/cantiknya-gunung-lawu-pagi-ini-puncaknya-tampak-bertopi, accessed June 2022.

[20] WC Skamarock, JB Klemp, J Dudhia, DO Gill, Z Liu, J Berner, W Wang, JG Powers, MG Duda, DM Barker and XY Huang. A description of the advanced research WRF model version 4. *Nat. Cent. Atmos. Res.* 2019; **145**, 550.

[21] JA Young. *Static stability.* Elsevier, Amsterdam, Netherlands, 2003.

[22] XW Bao and ZM Tan. Low-level vertical wind shear effects on the gravity wave breaking over an isolated two-dimensional orography. *Tellus Dyn. Meteorol. Oceanogr.* 2012; **64**, 17265.

[23] TL Clark and W Peltier. On the evolution and stability of finite-amplitude mountain waves. *J. Atmos. Sci.* 1977; **34**, 1715-30.

[24] B Klemp, J Dudhia and AD Hassiotis. An upper gravity-wave absorbing layer for NWP applications. *Mon. Weather Rev.* 2008; **136**, 3987-4004.

[25] I Colfescu, JB Klemp, MA Bollasina, SD Mobbs and RR Burton. The dynamics of observed lee waves over the snæfellsnes Peninsula in Iceland. *Mon. Weather Rev.* 2021; **149**, 1559-75.

[26] RF Hertenstein. The influence of inversions on rotors. *Mon. Weather Rev.* 2009; **137**, 433-46.

[27] RS Scorer. Theory of waves in the lee of mountains. *Q. J. Roy. Meteorol. Soc.* 1949; **75**, 41-56.

[28] RAF Denryanto and RH Virgianto. The impact of land cover changes on temperature parameters in new capital of Indonesia (IKN). *IOP Conf. Ser. Earth Environ. Sci.* 2021; **893**, 012033.
[29] MI Hastuti and JIA Paski. Assimilation of weather radar data using WRF 3DVar modelling for rainfall prediction. *IOP Conf. Ser. Earth Environ. Sci.* 2019; **303**, 012047.
[30] FP Sari, AP Baskoro and OS Hakim. Effect of different microphysics scheme on WRF model: A simulation of hail event study case in Surabaya, Indonesia. *AIP Conf. Proc.* 2018; **1987**, 020002.
[31] PJ Neiman and JA Shaw. Coronas and iridescence in mountain wave clouds over northeastern Colorado. *Bull. Am. Meteorol. Soc.* 2003; **84**, 1373-86.
[32] M Udina, J Bech, S Gonzalez, MR Soler, A Paci, JR Miró, L Trapero, JM Donier, T Douffet, B Codina and N Pineda. Multi-sensor observations of an elevated rotor during a mountain wave event in the Eastern Pyrenees. *Atmos. Res.* 2020; **234**, 104698.
[33] KR Chan, L Pfister, TP Bui, SW Bowen, J Dean-Day, BL Gary, W Fahey, KK Kelly, CR Webster and RD May. A case study of the Mountain Lee Wave Event of January 6, 1992. *Geophys. Res. Lett.* 1993; **20**, 2551-4.